Bifacial Peptide Nucleic Acid Directs Cooperative Folding and Assembly of Binary, Ternary, and Quaternary DNA Complexes

ARTICLE *in* BIOCHEMISTRY · AUGUST 2013

Impact Factor: 3.02 · DOI: 10.1021/bi4008963 · Source: PubMed

3 AUTHORS:

Xijun Piao
The Ohio State University
6 PUBLICATIONS **105** CITATIONS
SEE PROFILE

Xin Xia
The Ohio State University
6 PUBLICATIONS **23** CITATIONS
SEE PROFILE

Dennis Bong
The Ohio State University
32 PUBLICATIONS **1,141** CITATIONS
SEE PROFILE

BIOCHEMISTRY
including biophysical chemistry & molecular biology

Article

pubs.acs.org/biochemistry

Bifacial Peptide Nucleic Acid Directs Cooperative Folding and Assembly of Binary, Ternary, and Quaternary DNA Complexes

Xijun Piao, Xin Xia, and Dennis Bong*

Department of Chemistry and Biochemistry, The Ohio State University, 100 West 18th Avenue, Columbus, Ohio 43210, United States

Supporting Information

ABSTRACT: We report herein the structuring of single-stranded thymine-rich DNA sequences into peptide−DNA hairpin triplex structures via designed melamine−thymine nucleobase recognition. Melamine-displaying α-peptides were synthesized with the general form $(EM^*)_n$, where M* denotes a lysine residue side chain derivatized with melamine, a bifacial hydrogen bond complement for thymine. We have found that $(EM^*)_n$ peptides, which we term bifacial peptide nucleic acid (bPNA), function as a noncovalent template for thymine-rich DNA tracts. Unstructured DNA of the general form $dT_nC_mT_n$ are bound to $(EM^*)_n$ peptides and fold into cooperatively melting 1:1 bPNA−DNA hairpin complexes with dissociation constants in the submicromolar to low nanomolar range for $n = 4-10$. As the length of the interface (n) is decreased, the melting temperature of the bPNA−DNA complex drops significantly, though K_d increases are less substantial, suggestive of strong enthalpy−entropy compensation. This is borne out by differential scanning calorimetry analysis, which indicates enthalpically driven bPNA−DNA base-stacking that becomes markedly less exothermic as the recognition surface n decreases in size. The recognition interface tolerates a high number of "mismatches" and indicates half-site, or monofacial, recognition between melamine and thymine may occur if only 1 complementary nucleobase is available. Association correlates directly with fractional thymine content, with optimal binding when the number of T−T sites match the number of melamine units. Interestingly, when a DNA host has more T−T sites than melamine sites on bPNA, two or three bPNAs can bind to a single DNA, resulting in ternary and quaternary complexes that have higher thermal stability than the binary (1:1) bPNA−DNA complex, suggestive of cooperative multisite binding. In contrast, when two bPNAs of different lengths bind to the same DNA host, a ternary complex is formed with two melting transitions, corresponding to independent melting of each bPNA component from the complex. These data demonstrate that melamine-displaying bPNA recognize thymine-rich DNA in predictable and multifaceted ways that allow binding affinity, structure stability, and stoichiometry to be tuned through simple bPNA length modification and matching with DNA length. Synthetic bPNA structuring elements may be useful tools for biotechnology.

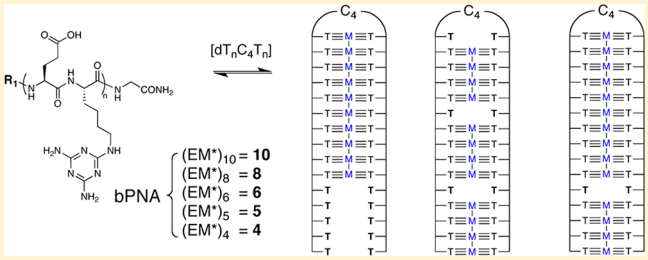

Nucleic acid triplex formation commonly involves Hoogsteen base-pairing of single-stranded oligonucleotides to preformed duplex structures, often under non-physiological pH and salt conditions. The discovery of triplex DNA structures[1] has inspired decades of research aimed at understanding triplex formation[2,3] as well as chemical methods for targeting[4−8] the information presented in duplex DNA. We recently reported[9] an alternative strategy for a new class of heterotriplex formed from synthetic peptides and homopyrimidine DNA that does not require any prior secondary structure. Two noninteracting, unstructured thymine-rich DNA strands are brought together on a bridging bifacial melamine-displaying peptide nucleic acid (bPNA) template strand to form a cooperatively folded 1:2 bPNA−DNA triplex via melamine−thymine recognition. This concept is similar to the targeting of short, single-stranded oligopurines with pyrimidine "clamps" or cyclic DNA reported by Hélène and Kool,[10] intramolecular DNA triplexes,[3] and synthetic "Janus-wedge" bifacial nucleobase mimics,[2,11−13] with the distinction that no prior secondary structure, covalent cyclization, or high concentration of Mg^{2+} is required. Unlike conventional PNA with a non-native polypeptide backbone and native nucleobase content, bPNA has an α-peptide structure derived from native amino acids and a non-native bifacial melamine nucleobase mimic. Bifacial PNA may also be operationally distinguished from conventional PNA in that bPNA is an *associative* agent that brings noninteracting oligothymidine DNA strands together in 1:2 bPNA−DNA triplex, whereas PNA is often used as a *dissociative* agent that invades existing nucleic acid (NA) duplexes to produce 2:1 PNA−NA triplex hybrids.[14−17] Bifacial PNA is an artificial peptide strand that binds and folds a DNA partner through the use of melamine as a synthetic nucleobase-mimic that hydrogen bonds with two thymine bases on their Watson−Crick faces (Figure 1). Bifacial guanine−guanine nucleobase interactions exist natively in G-quadruplexes;[18] accordingly, guanine-rich

Received: July 9, 2013
Revised: August 18, 2013

   dx.doi.org/10.1021/bi4008963 | *Biochemistry* XXXX, XXX, XXX−XXX

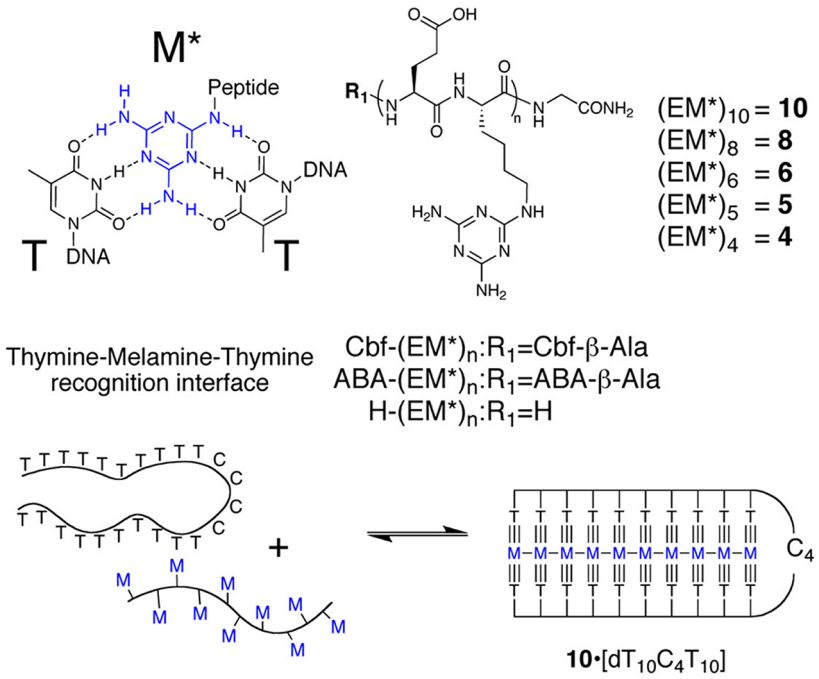

Figure 1. Illustration of melamine–thymine interaction directing DNA and bPNA assembly. (Top) The structure of the $(EM^*)_n$ peptides (bPNA) with N- and C–Terminating groups is shown. Cbf = 5(6)-carboxyfluorescein, ABA = 4-acetamidobenzamide. (Bottom) A schematic of a 1:1 hairpin triplex structure formed from unstructured **10** and $dT_{10}C_4T_{10}$.

PNA can bind to two G-rich DNA strands to form 1:1 heteromeric PNA–DNA G-quadruplex structures[19] as well as PNA-only quadruplex structures.[20] Unlike G-quartets and DNA triplexes, melamine bPNA does not self-assemble, utilize Hoogsteen base-pairing, or require direct interactions between DNA strands and instead targets unstructured T-tracts for binding. It is anticipated that this artificial recognition strategy could be a general method for triggered folding of oligothymidine containing nucleic acids into synthetic stem-loops. As is well documented by studies on native and designed riboswitches, chemically triggered structuring of nucleic acid tracts may be utilized to control biological functions when coupled to gene regulatory elements.[21−23] The melamine bPNAs are easily prepared via reaction of the ε-amino group of lysine with diaminochlorotriazine to yield an amino acid derivative for standard solid-phase peptide synthesis.[24] The facility of direct amino substitution on chlorotriazine rings has led to considerable investigation of melamine as a diversity platform for combinatorial chemistry and dendrimer synthesis,[25,26] and triazines themselves have been suggested as products of prebiotic chemistry,[27−30] forming readily from cyano derivatives.[31−35] Indeed, Eschenmoser and Krishnamurthy prepared peptide/peptoid displayed triazines[32,33] that interface with native DNA/RNA to form duplexes, and facile synthesis of triazine-derived nucleosides was shown by Siegel and Tor.[31] A detailed study is presented on the biophysical underpinnings and scope of melamine-displaying peptides that can cooperatively bind and structure single-stranded thymine-rich DNA into higher order triplex structures.

The synthetic triaminotriazine (melamine) provides a divalent site for thymine recognition when monoderivatized on an exocyclic nitrogen. Melamine and its derivatives have been extensively studied in organic solvents and the solid-state as an assembly partner for cyanuric acid derivatives,[36−38] and more recently in aqueous-phase assemblies.[39−51] Heterocycle recognition of melamine and cyanurates is directed by hydrogen bond recognition, but driven by exothermic base-stacking akin to DNA-recognition.[48] Co-crystallization of melamine with thymine, uracil, and 5-fluorouracil[46] from aqueous solution provided structural evidence of the expected multifacial hydrogen bonding patterns between triazine and nucleobase in the solid state, whereas Baranger and Zimmerman had established the ability of melamine–acridine conjugates to selectively intercalate into T–T and U–U mismatch sites in solution,[52,53] indicative of bifacial melamine recognition. Robust exothermic binding of 5-fluorouracil to polyacrylate-displayed melamine was found to trigger condensation of soluble polymer into 5-FU loaded nanoparticles, suggesting that melamine–cyanurate type recognition may be generally extended to include interactions with thymine/uracil.[46] In addition, Eschenmoser and Krishnamurthy have demonstrated that diaminotriazine-displaying α-peptides function as novel PNAs that form stable peptide–DNA and RNA duplexes.[32,33] We speculated that replacement of the aliphatic CH_2 linkage to the heterocycle in diaminotriazine with an NH to yield a triaminotriazine (melamine) side chain derivative would create a bifacial recognition nucleus for thymine and switch the assembly to triplex structures. This was borne out by our studies on the binding of melamine-derivatized peptides with dT_{10} tracts.[9] We found that α-peptides presenting ten melamine-derivatized lysine (M*) and glutamic acid (E) residues at alternate positions recognize unstructured single-stranded decathymidine tracts and induce cooperative folding into $(EM^*)_{10}$–DNA triplex structures of 1:2 peptide–DNA stoichiometry. Glutamic acid residues provide solubility and create a repulsive electrostatic interaction with DNA upon ionization, thus minimizing potential nonspecific binding. Connection of dT_{10} tracts with a noninteracting dC_{10} linker yielded a peptide–DNA complex of 1:1 ratio, consistent with the formation of a DNA hairpin structure with a peptide–dT_{10}

dx.doi.org/10.1021/bi4008963 | *Biochemistry* XXXX, XXX, XXX–XXX

triplex stem and dC_{10} single-stranded loop. Herein, we focus our examination on melamine−thymine driven assembly of peptide−DNA complexes as a function of interface length in the context of the hairpin-triplex stem motif. The dependence of peptide−DNA binding on the length of the interface was investigated by synthesis of $(EM^*)_n$ peptides, which we term herein as bifacial peptide nucleic acid (bPNA), with n = 4−6, 8, and 10 (Figure 2). These peptides bound to their $dT_nC_4T_n$ partners with the expected 1:1 hairpin triplex stoichiometry, and complex stability decreased with n. Notably, length matching of the DNA and peptide was critical in determining stoichiometry; longer DNA strands were found to host more than one peptide, supporting the notion that a single melamine repeat unit (EM*) is required to interact with each T−T pair.

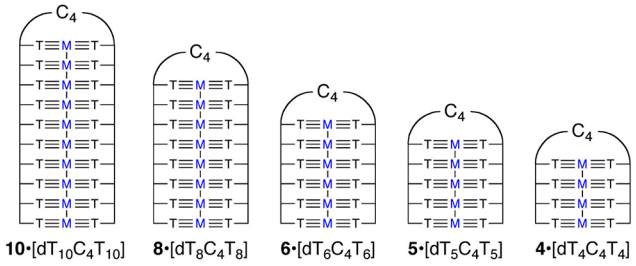

Figure 2. Structures of 1:1 binary hairpin complexes between $(EM^*)_n$ bPNA and their corresponding $T_nC_4T_n$ DNA partners.

EXPERIMENTAL SECTION

General Information. All DNA was purchased from Sigma-Aldrich and used as provided. Peptides were synthesized using standard solid phase peptide synthesis (SPPS) with Fmoc chemistry and purified to homogeneity on HPLC, and their identity was verified by MALDI-MS. Melamine-derivatized lysine (Fmoc−Lys(melamine)−OH) was synthesized as previously reported and used in SPPS without side chain protection. All measurements were carried out in triplicate using Dulbecco's phosphate buffered saline (DPBS) at pH 7.4 without additional salt. Each peptide−DNA sample was incubated at 37 °C for one hour then cooled to 25 °C over one hour prior to measurement except where noted. Peptides and DNA concentrations were calculated from stock solutions using UV absorbance derived from melamine, ninhydrin test, ABA, Cbf, or nucleobases as appropriate.

Peptide−DNA Titration and Binding Isotherms. Fluorescence quenching experiments were performed on a Perkin-Elmer luminescence spectrometer (LS-50B) equipped with a PTP-1 temperature programmer. Concentration of all peptides in fluorescence quenching titration experiments to determine binding stoichiometry was 1 μM. Fluorescence anisotropy (from Cbf−$(EM^*)_n$) based binding isotherms were measured on a Molecular Devices Spectramax M5. All binding isotherms were carried out at 25 nM peptide at 25 °C with the exception of Cbf-4 binding to $dT_4C_4T_4$, which was carried out at 400 nM peptide at 8 °C on the LS-50B; samples were incubated in an ice bath for 1 h prior to measurement.

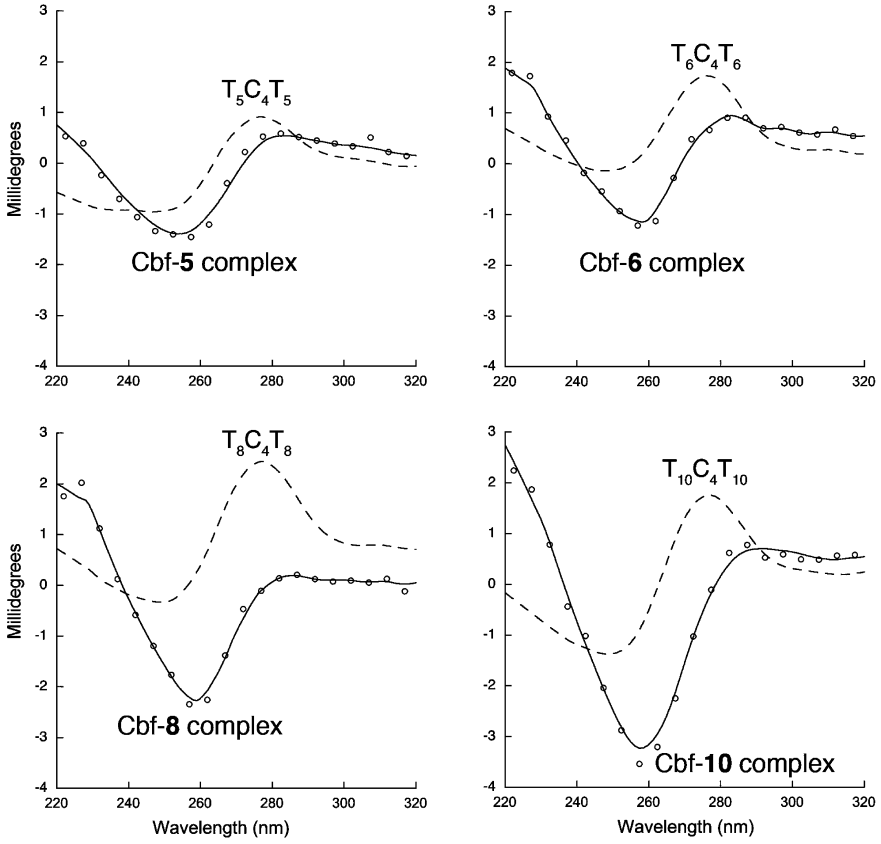

Figure 3. CD spectra of single-stranded $dT_nC_4T_n$ DNA (---) and the corresponding Cbf−$(EM^*)_n$ bPNA complex, as labeled (—). All DNA and bPNA−DNA complexes are at 5 μM concentration; all bPNAs exhibit a neglible CD signal under these conditions.

dx.doi.org/10.1021/bi4008963 | Biochemistry XXXX, XXX, XXX−XXX

Melting Experiments. All measurements were carried out with a temperature change rate of 1 °C per minute. Peptide–DNA complex melting was followed by UV absorbance changes on a Cary-100 UV–vis spectrophotometer equipped with an air-circulating temperature controller. Peptide–DNA complex concentration was 5 μM for all UV samples. All DSC samples were measured on a Microcalorimeter VP-DSC at 25 μM peptide/DNA concentration with exceptions as noted. The average of at least three upscans is presented; the average of three downscans is also presented for selected complexes.

RESULTS AND DISCUSSION

1:1 bPNA–DNA Complexes. Melamine-derivatized α-peptides of varying length were prepared as previously reported.[9] Briefly, the ε-amine of Boc-lysine was reacted with diaminochlorotriazine to form a side chain coupled melamine ring following chloride displacement. Conversion of the Boc group to Fmoc furnished an Fmoc–Lys(melamine)–OH amino acid derivative for use in standard solid phase peptide synthesis. The melamine side chain did not require protection from coupling and resin cleavage conditions. Peptides (bPNA) were prepared with the general form $(EM^*)_n$, wherein M* represents the melamino–lysine residue and E represents glutamic acid. Glutamic acid was chosen to occupy alternate positions to achieve the pattern shown by Eschenmoser[32,33] and Ghadiri[30] to yield duplex DNA/RNA structures with α-peptides. Furthermore, the acidic side chains are expected to be largely ionized at neutral pH, minimizing nonspecific electrostatic binding effects to DNA and mimicking the electrostatically repulsive backbone strand interactions found in native DNA duplexes and triplexes. Peptides with 4–10 repeat units were prepared and were N-terminally acylated with carboxyfluorescein dye or acetamidobenzoic acid (ABA) or left with a free N-terminus. If capped, then a β-alanine residue was used as a linker between the chromophore and the recognition interface.

Formation of $T_nC_4T_n$:$(EM)_n$ Complexes. The fluorescent Cbf–$(EM^*)_n$ bPNA were well suited for determination of stoichiometry of interaction and dissociation constant with their $dT_nC_4T_n$ partners. As previously reported,[9] DNA complexation of labeled bPNA resulted in both fluorescence quenching as well as increased fluorescence anisotropy. These measurements were applied at high (saturating, micromolar) and low (low to midnanomolar) concentration regimes to determine stoichiometry and binding constants, respectively. Clear 1:1 complexation with $dT_nC_4T_n$ DNA is observed within the Cbf–$(EM^*)_n$ series (n = 4–6, 8, 10) with the exception of Cbf-**4**. This shortest bPNA exhibits the weakest binding, making it difficult to obtain saturating conditions and clear stoichiometry determination (Supporting Information). All bPNA induce a structural change in the DNA, as qualitatively judged by circular dichroism (Figure 3, Supporting Information). CD spectral changes upon bPNA binding were similar for all peptides, though longer DNA exhibited more intense signals. As previously reported with bPNA complexation of $dT_{10}C_{10}T_{10}$, a large positive Cotton effect at ~280 nm corresponding to unstructured DNA was transformed into a strong negative CD peak at 260 nm. All bPNA–DNA complexes exhibited a cooperative thermal melting curve by UV absorbance or fluorescence quenching analysis (Figure 4), with the melting temperatures (T_m) correlated with repeat unit (n).

Binding Affinity and Enthalpy of bPNA–DNA Complexes. Fluorescence anisotropy derived binding isotherms

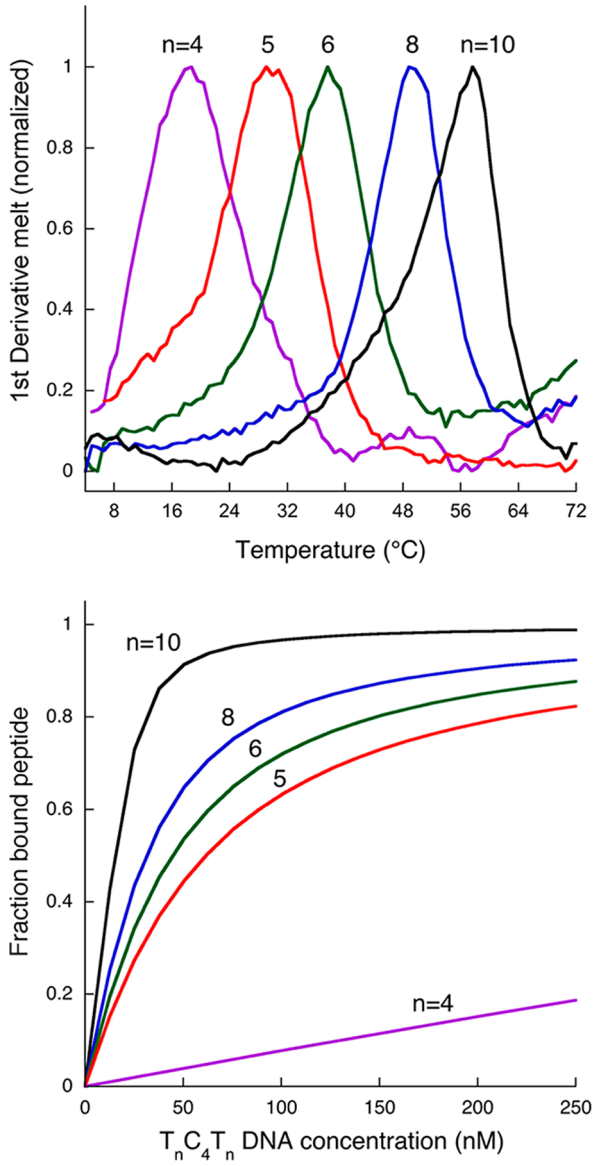

Figure 4. (Top) Normalized first derivatives of thermal melts (UV) of the 1:1 $(EM^*)_n$ bPNA complexes with the matching $dT_nC_4T_n$ DNA, with n as indicated at 5 μM bPNA concentration. (Bottom) Binding isotherms of complex formation fit to a 1:1 binding model ($R^2 \geq 0.96$), with n as indicated. bPNA concentration is 25 nM.

were produced from the treatment of Cbf–$(EM^*)_n$ bPNA with DNA ($dT_nC_mT_n$) and fit to a 1:1 binding model to acquire dissociation constants (K_d). As expected on the basis of qualitative inspection and T_m trends, longer recognition interfaces yielded tighter DNA binding and lower K_d. The longest bPNA (n = 10) yielded a K_d of ~2.6 nM on binding $dT_{10}C_4T_{10}$, exhibiting similar affinity as previously reported with a longer dC loop ($dT_{10}C_{10}T_{10}$). Although the K_d trend (Table 1) showed incremental loss in affinity with reduction of recognition interface, heat of binding and T_m decreased drastically as the complexes were shortened, with T_m ranging from 57 °C for Cbf–$(EM^*)_{10}$ to below room temperature (19 °C) for Cbf–$(EM^*)_4$. Although the heat required to dissociate bPNA **10** from $dT_{10}C_4T_{10}$ (294 kcal/mol) indicates a binding interaction that is roughly 50% more enthalpically favorable per triplex layer than found in the formation of an intramolecular TAT DNA triplex,[3] ΔH_d steadily decreases with interface size

dx.doi.org/10.1021/bi4008963 | *Biochemistry* XXXX, XXX, XXX–XXX

Table 1. Thermodynamic Data for $[(EM^*)_n \cdot dT_nC_4T_n]^a$

bPNA–DNA 1:1 complex	K_d (nM)	T_m (°C)	ΔG_d	ΔH_d	ΔS_d
10·$dT_{10}C_4T_{10}$	2.6 ± 0.4	57	11.7	293	946
8·$dT_8C_4T_8$	18.7 ± 1.7	49	10.4	247	793
6·$dT_6C_4T_6$	32.1 ± 3.8	38	10.2	127	392
5·$dT_5C_4T_5$	49.9 ± 4.6	29	9.9	60	167
4·$dT_4C_4T_4$	~1000	19	7.8		

[a]Data for dissociation are shown. ΔG_d and ΔH_d of dissociation are shown in kcal/mol and ΔS_d of dissociation is shown in cal/(mol K). Apparent K_d based on mass balance for **4** is shown.

until it can no longer be detected when **4** binds to $dT_4C_4T_4$ (Figure 5, Table 1). As with the PNA–DNA, DNA–DNA, and

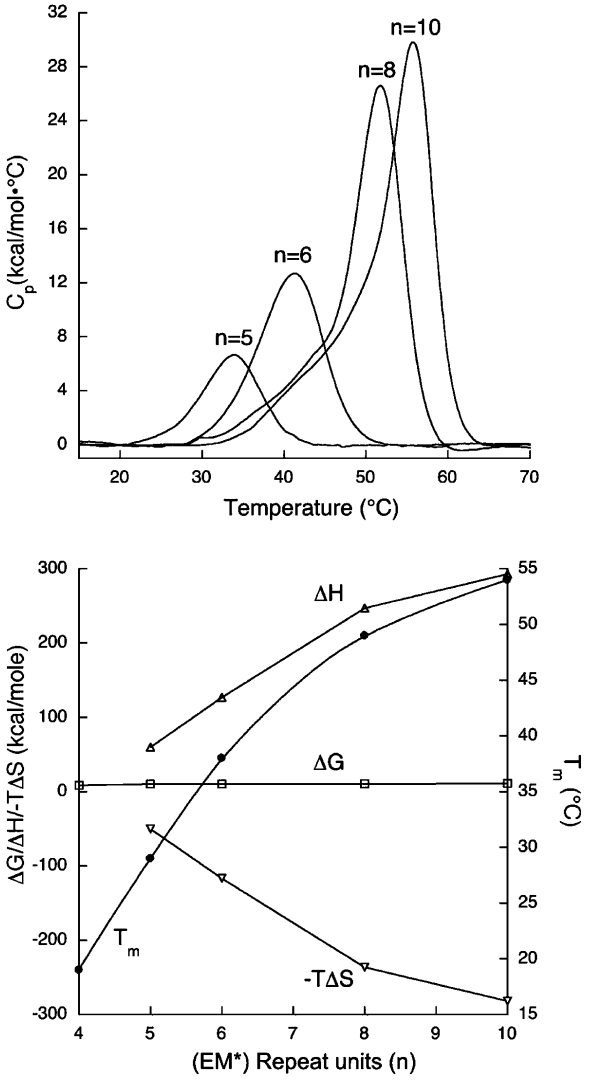

Figure 5. (Top) DSC upscans of 1:1 complexes of $(EM^*)_n \cdot dT_nC_4T_n$, with n as labeled. (Bottom) Thermodynamic parameters for complex dissociation (as labeled) and T_m (●) on the right axis as a function of repeat unit.

melamine–cyanurate assemblies, bPNA–DNA recognition[9] is enthalpically driven.[3,10,54,55] Near perfect enthalpy–entropy compensation is observed as the length of the interface is varied, with both heat of binding and entropic cost of assembly sharply decreasing with the number of (EM*) repeat units (Figure 5).[56,57] The enthalpic benefit of peptide–DNA binding vanishes with an (EM*) repeat of four, as reflected in significant loss of DNA affinity (Figure 4) as bPNA length is decreased from **5** to **4**. A plot of ΔH_d vs T_m for the $(EM^*)_n$ peptides binding to their $dT_nC_4T_n$ DNA partners reveals a linear relationship (Figure 6) that predicts that complex assembly with T_m around room temperature should be enthalpically neutral (ΔH_d = 0), as is observed for [**4**·$dT_4C_4T_4$] with T_m = 19 °C. The association of the peptide–DNA complex [**4**·$dT_4C_4T_4$] has a weak enthalpic signature below DSC detection limits, but may be readily observed by thermal melt (UV) and fluorescence anisotropy measurements.

Tolerance of "Mismatch" Sites in $(EM^*)_{10}$ DNA Complexation. Although selectivity of $(EM^*)_{10}$ bPNA for thymine-rich DNA relative to the other native DNA nucleobases has been previously established, the tolerance of nonthymine nucleobases at the recognition interface was unknown. We tested the affinity of Cbf-**10** for a series of 24 nucleotide DNAs based on $dT_{10}C_4T_{10}$, as a function of thymine content, systematically punctuating the dT_{10} tracts with cytidine nucleotides. Eighteen DNA binding partners for Cbf-**10** with thymine content decreasing relative to $dT_{10}C_4T_{10}$ were evaluated by T_m measurement to assay the effect of a melamine "mismatch," or non-T site (Table 2). Notably, complex formation was detectable even with 40% replacement of T for C, though thermal stability dropped to ~19 °C with this high number of mismatches. Thermal stability of the complexes showed good linear correlation with thymine content (Figure 6). Selected low melting complexes were studied by fluorescence quenching titration to confirm that the 1:1 peptide:DNA stoichiometry of a hairpin triplex, despite the high number of mismatches (Supporting Information). Inspection of complex T_m as a function of T → C substitution strongly support the notion that the melamine side chains of Cbf-**10** prefer binding to antiparallel T–T sites but can bind to single thymine half-sites, presented as T–C or C–T mismatch sites formed when the 24-nt DNA is folded into a hairpin structure. Indeed, two T → C substitutions that yield half-sites (entry 3, T_m = 54.1 °C) are more thermally stable than substitutions that do not (entry 5, T_m = 49.8 °C). This effect may also be observed when comparing entries 6 and 11, which have identical thymine fraction (67%) yet are separated by 6 °C in melting temperature. Again, the higher melting complex formed in entry 6 distributes the T → C substitutions exclusively into half-sites (T–C, C–T pairs), whereas entry 11 presents two contiguous C–C mismatch sites, effectively dividing the original dT_{10} tract into two T_4 tracts separated by CC linkers. Similarly, the favorable presence of T–C, C–T half-sites is seen when comparing entries 12 and 14, both of which are 58% T. Thus, it appears that clustered T → C substitutions are more damaging to bPNA recognition than distributed substitutions; the latter pattern allows the entire peptide to participate in full site (T–T) or T–C and C–T half-site recognition. An exception is found at 50% thymine content (entries 16–18), where a block of four C–C mismatch sites is preferred (T_m = 25.6 °C) over a system with eight distributed half-sites (entry 17, T_m = 19.6 °C) or four distributed C–C mismatches (entry 18, T_m = 18.7 °C.) This observation may be understood if one considers that a cluster of mismatch sites also yields flanking clusters of uninterrupted T_3 tracts, allowing a preferred binding mode to operate. With a total of six T–T sites, Cbf-**10** binding to entry 16 is analogous to the [Cbf-**6**·$dT_6C_4T_6$] complex (Table 1), which in fact has much higher thermal stability (T_m = 38 °C). Lower thermal stability relative

dx.doi.org/10.1021/bi4008963 | *Biochemistry* XXXX, XXX, XXX–XXX

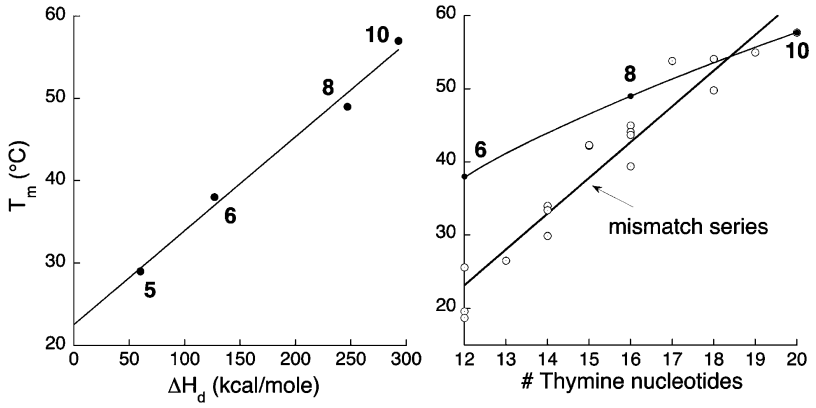

Figure 6. (Left) T_m dependence of bPNA–DNA complexes $[(EM^*)_n{\cdot}T_nC_4T_n]$ as labeled on heat of dissociation (from DSC). A linear fit (R^2 = 0.99) is shown with T_m = 21.5 °C + 0.11ΔH. (Right) T_m dependence on thymine content of (○) Cbf-**10** complexes with DNA shown in Table 2 and of (●) $[(EM^*)_n{\cdot}T_nC_4T_n]$ complexes as labeled.

Table 2. T_m of Cbf-10 complexes with T-rich 24 nt DNA

entry	DNA Sequences	T_m /°C	#thymine bases
1	5'-TTTTTTTTTT 3'-TTTTTTTTTT)C4	57.7	20
2	5'-TTTTTTTTTT 3'-TTTTTCTTTT)C4	55.0	19
3	5'-TTTTTTCTTT 3'-TTTTTCTTTT)C4	54.1	18
4	5'-TTCTTTTCTT 3'-TTTTTCTTTT)C4	53.8	17
5	5'-TTTTTCTTTT 3'-TTTTTCTTTT)C4	49.8	18
6	5'-TCTTCTTCTT 3'-TTTTTCTTTT)C4	45.0	16
7	5'-TTCTTTTCTT 3'-TTTCTTCTTT)C4	44.1	16
8	5'-TTCTTTCTTT 3'-TTCTTTCTTT)C4	43.7	16
9	5'-TTCTCTCTCT 3'-TTTTTCTTTT)C4	42.3	15
10	5'-TCTTCTTCTT 3'-TTTCTTCTTT)C4	42.2	15
11	5'-TTTTCCTTTT 3'-TTTTCCTTTT)C4	39.4	16
12	5'-TCTTCTTCTT 3'-TTTCTTCTCT)C4	34.0	14
13	5'-TTCTTCTTCT 3'-TTCTTCTTCT)C4	33.4	14
14	5'-TTTTCCCTTT 3'-TTTTCCCTTT)C4	29.9	14
15	5'-TTCTCTCTCT 3'-TTTCTCTCTT)C4	26.5	13
16	5'-TTTCCCCTTT 3'-TTTCCCCTTT)C4	25.6	12
17	5'-TTCTCTCTCT 3'-TCTCTCTCTT)C4	19.6	12
18	5'-TTCTCTCTCT 3'-TTCTCTCTCT)C4	18.7	12

to $[\mathbf{6}{\cdot}dT_6C_4T_6]$ may be a result of the greater entropic cost of complexing larger macromolecules with more degrees of freedom, as well as a "dangling end" effect in which the terminal bases are not buried on both sides of the T-tract in entry 16.[54]

Interface Length Mismatch and Higher Order Assembly. The clear dependence of complex stability on the melamine–thymine interface length coupled with our studies on mismatch tolerance suggested that it might be possible to select assembly order on the basis of length matching. We set out to test this notion through the study of bPNA–DNA complexes in which the melamine repeat unit was not identical to the number of T–T pairs. The DNA sequence $dT_{18}C_4T_{18}$ was studied as a host for the Cbf–$(EM^*)_n$ series of peptides where it was expected that 1:1 bPNA–DNA complexes would not result in saturation of the 18 available T–T sites (Figure 7).

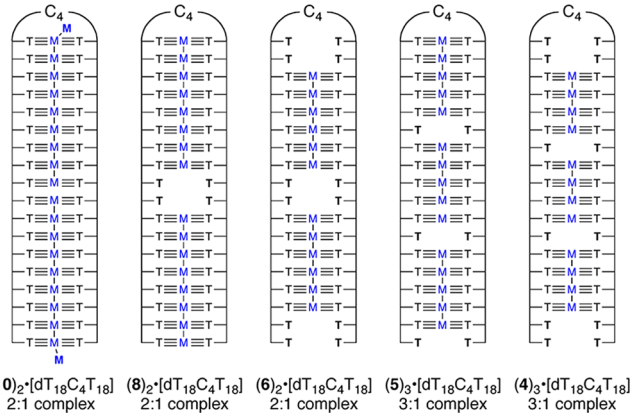

Figure 7. Proposed hairpin multiplex structures formed from complexation of 2 or more Cbf–$(EM^*)_n$ peptides to a $dT_{18}C_4T_{18}$ template. Stoichiometries were determined by fluorescence quenching titration experiments.

Fluorescence quenching experiments indicated higher order peptide–DNA complexes were formed for all peptides Cbf-**4** to Cbf-**10** (Table 3 and Supporting Information). Gratifyingly, the altered stoichiometry correlated closely with a 1:1 match of melamine groups with T–T pairs; peptides Cbf-**10**, Cbf-**8**, and Cbf-**6** formed ternary complexes with $dT_{18}C_4T_{18}$ at a 2:1 bPNA–DNA ratio. Size selection was demonstrated by

Table 3. T_m's of Higher Order Peptide–DNA Complexes[a]

bPNA	DNA	bPNA:DNA	transition	T_m (°C)
10	$dT_{18}C_4T_{18}$	2:1	single	60
8	$dT_{18}C_4T_{18}$	2:1	single	55
6	$dT_{18}C_4T_{18}$	2:1	single	48
5	$dT_{18}C_4T_{18}$	3:1	single	39
4	$dT_{18}C_4T_{18}$	3:1	single	30
4	$dT_{10}C_4T_{10}$	2:1	single	25

[a]UV melting experiments were performed at 5 μM DNA at the specified bPNA–DNA stoichiometry with Cbf–bPNA.

dx.doi.org/10.1021/bi4008963 | *Biochemistry* XXXX, XXX, XXX–XXX

formation of 3:1 bPNA–DNA quaternary complexes with Cbf-**5** and Cbf-**4**. This pattern suggests that at least two melamine sites are not bound in the Cbf-**10** 2:1 complex with $dT_{18}C_4T_{18}$ and that the remaining multimeric complexes do not saturate all possible T–T sites on the DNA template. It is expected that two equivalents of Cbf-**8**, with eight melamine repeat units each, would leave two melamine binding sites unsaturated in a 2:1 bPNA–DNA complex, whereas a 3:1 complex would leave six melamine units unbound. It appears that the enthalpic gain of binding two melamine units likely does not outweigh the entropic cost of forming a quaternary complex, and thus, a ternary $[(\text{Cbf-}\mathbf{8})_2{\cdot}dT_{18}C_4T_{18}]$ is observed instead. This calculation similarly favors the formation of a $[(\text{Cbf-}\mathbf{10})_2{\cdot}dT_{18}C_4T_{18}]$ ternary complex rather than a 1:1 assembly, because eight additional melamine repeats can be bound to offset the entropic cost of a higher order assembly. It is notable that Cbf-**6** binds at a 2:1 rather than a 3:1 peptide–DNA ratio as the number of melamine repeats in three Cbf-**6** peptides matches exactly the number of T–T sites available. This is possibly due to steric clash caused by carboxyfluorescein N-termination at a DNA-binding position; there may not be enough space along the DNA template to accommodate three fluorescent dyes as well as melamine/T–T binding site saturation, thus favoring formation of a 2:1 peptide–DNA complex instead. All of these higher order bPNA–DNA complexes melt cooperatively with a single transition and a significant increase in T_m is observed relative to the 1:1 complexes. The effect is strongest for the more weakly binding shorter bPNA: Cbf-**4**, Cbf-**5**, and Cbf-**6** exhibit a ~10 °C increase in thermal stability, whereas smaller increases of 6 and 3 °C are observed for the 2:1 ternary complexes with Cbf-**8** and Cbf-**10**. These stability increases are indicative of strongly cooperative multiplex binding, wherein the ternary or quaternary complex melts in a single transition that releases all bound peptides at once without detectable intermediate complexes.

Length Matching Directs Heterotriplex Formation. Length matching recognition selectivity was tested using a slightly shorter DNA template, $dT_{15}C_4T_{15}$. This DNA template was designed to be too short to accommodate more than a single Cbf-**10** peptide but long enough to display unoccupied T–T sites. Notably, although CD measurements of the $[\text{Cbf-}\mathbf{4}{\cdot}dT_4C_4T_4]$ complex yielded weak signals of secondary structural changes in the DNA, titration of the peptide to form the quaternary complex $[(\text{Cbf-}\mathbf{4})_3{\cdot}dT_{15}C_4T_{15}]$ was accompanied by obvious DNA folding with an isodichroic point indicative of a single transition, as observed on thermal melt (Figures 9 and 10). Fluorescence quenching titration confirmed that the T_{15} tracts were not long enough to permit a 2:1 peptide–DNA complex with Cbf-**10**, yielding a 1:1 stoichiometry instead. A similar titration with Cbf-**4** and $dT_{15}C_4T_{15}$ indicated that a 3:1 peptide–DNA binding was maintained even after reduction of T–T sites. Replacement of the fluorophore with ABA on peptide **10** permitted the formation of a 1:1 complex between ABA-**10** and $dT_{15}C_4T_{15}$ that would be spectroscopically invisible in a fluorescence quenching based titration with Cbf-**4**. The $[\text{ABA-}\mathbf{10}{\cdot}dT_{15}C_4T_{15}]$ complex would thus be preorganized to accept an additional peptide binding partner in the five unbound T–T sites. Gratifyingly, fluorescence quenching titration of Cbf-**4** against preformed $[\text{ABA-}\mathbf{10}{\cdot}dT_{15}C_4T_{15}]$ revealed a clear transition to a 1:1 stoichiometry of interaction with the complex, providing evidence for formation of a 1:1:1 complex of $[\text{ABA-}\mathbf{10}{\cdot}\text{Cbf-}\mathbf{4}{\cdot}dT_{15}C_4T_{15}]$ (Figures 8 and 9). This

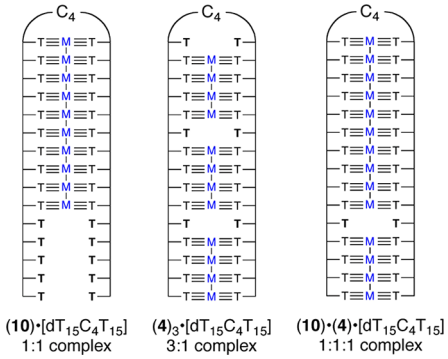

Figure 8. bPNA–DNA hairpin structures formed from complexation of $dT_{15}C_4T_{15}$ to 1 equiv of Cbf-**10** alone and to 3 equiv of Cbf-**4** alone and a 1:1:1 complex formed from ABA-**10**, Cbf-**4**, and $dT_{15}C_4T_{15}$.

assembly, wherein peptides of two different lengths are bound to a single DNA template, exhibits two distinct melting transitions that may be assigned to the separate thermally driven dissociations of the two peptides (Figure 9). This finding stands in contrast to the bPNA–DNA multiplexes formed when two or more copies of the same peptide are bound to one DNA molecule, which melt cooperatively in a single transition with elevated T_m. Analysis of the thermal melt reveals transition temperatures that are similar to the T_m's observed with the heterodimeric peptide–DNA mixtures. It appears that the Cbf-**4** peptide is thermally dissociated first at about 29 °C, and the remaining $[\text{ABA-}\mathbf{10}{\cdot}dT_{15}C_4T_{15}]$ complex melts at 60 °C. It is not clear why the first transition temperature is elevated in a manner similar to the cooperative melting of $[(\text{Cbf-}\mathbf{4})_3{\cdot}dT_{15}C_4T_{15}]$ because Cbf-**4** melts independently of the ABA-**10** in the heterotrimer. It is possible that DNA template preorganization by ABA-**10** binding reduces the entropic cost of docking the shorter Cbf-**4** peptide, thus increasing thermal stability. Further investigation by DSC revealed the expected enthalpically favorable assembly signatures previously observed in the length-matched $[(EM^*)_n{\cdot}dT_nC_4T_n]$ systems, with some remarkable differences. Dissociation of $[\text{ABA-}\mathbf{10}{\cdot}dT_{15}C_4T_{15}]$ required 281 kcal/mol, similar to what was observed on analysis of $[\text{Cbf-}\mathbf{10}{\cdot}dT_{10}C_4T_{10}]$ by DSC (293 kcal/mol). The heterotrimer $[\text{ABA-}\mathbf{10}{\cdot}\text{Cbf-}\mathbf{4}{\cdot}dT_{15}C_4T_{15}]$ exhibited two melting transitions with absorption of 6 kcal/mol in the first transition, followed by 294 kcal/mol in the second transition (Figure 9). These findings are again consistent with the binary, length-matched $[(EM^*)_n{\cdot}dT_nC_4T_n]$ systems, wherein $[\text{Cbf-}\mathbf{4}{\cdot}dT_4C_4T_4]$ melting did not yield detectable heat transfer; thus, a modest but detectable improvement in Cbf-**4** binding could account for the 6 kcal/mol absorbance in the DSC spectrum. DNA folding and triplex formation with a tightly binding peptide ligand such as **10** generates a preformed site for a shorter peptide. Although there is enthalpic benefit to complexation of the shorter peptide **4**, it is decoupled from the binding of the longer peptide ligand **10**, as the structure can be independently folded with **10** alone. The interaction of the weakly binding peptide **4** with the $dT_{15}C_4T_{15}$ scaffold reveals strong avidity effects, exhibiting half-saturation of peptide binding (apparent K_d by mass balance) at 250 nM DNA as compared to 1150 nM DNA for the $dT_4C_4T_4$ system (Figure 10). Calorimetric analysis of $[(\text{Cbf-}\mathbf{4})_3{\cdot}dT_{15}C_4T_{15}]$ yielded the most striking finding: 330 kcal heat per mole of DNA was absorbed on complex dissociation! Thus, although the enthalpic benefit of base-stacking 4 triplex layers only weakly

dx.doi.org/10.1021/bi4008963 | *Biochemistry* XXXX, XXX, XXX–XXX

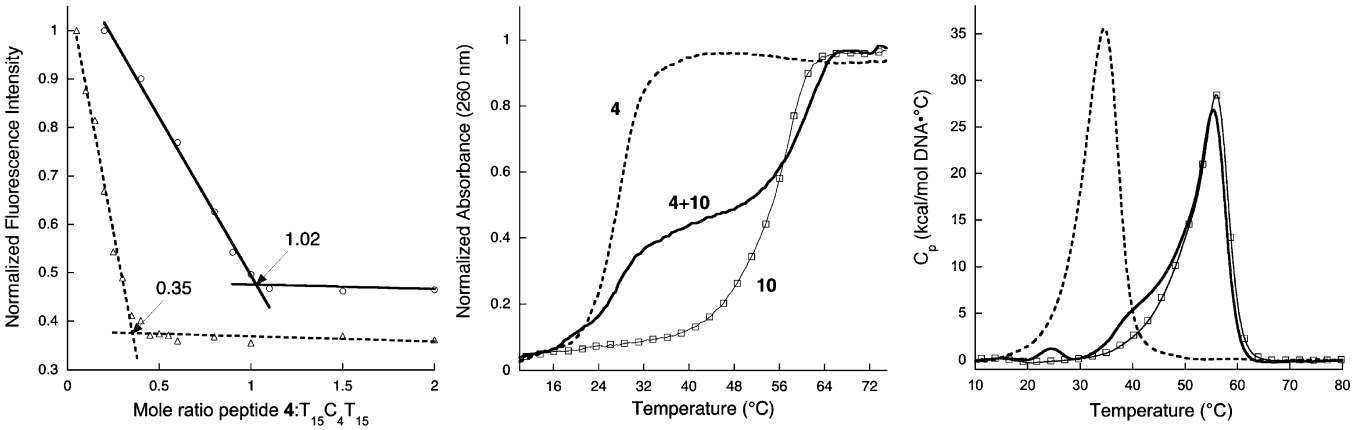

Figure 9. Analysis of binary and ternary complexes of $dT_{15}C_4T_{15}$, with peptides Cbf-**4** and ABA-**10**, labeled as follows: (---) = $[(\mathbf{4})_3{\cdot}dT_{15}C_4T_{15}]$, (□) = $[\mathbf{10}{\cdot}dT_{15}C_4T_{15}]$, and (—) = $[\mathbf{10}{\cdot}\mathbf{4}{\cdot}dT_{15}C_4T_{15}]$. (Left) Normalized fluorescence quenching plots indicating stoichiometry of binding of Cbf-**4** as a function of increasing $dT_{15}C_4T_{15}$ DNA (---) and as a function of increasing preformed [ABA-**10**· $dT_{15}C_4T_{15}$] complex (—). (Center) UV melts of $dT_{15}C_4T_{15}$ complexes, as labeled. (Right) Differential scanning calorimetry (upscans only) of the binary and ternary complexes of $dT_{15}C_4T_{15}$.

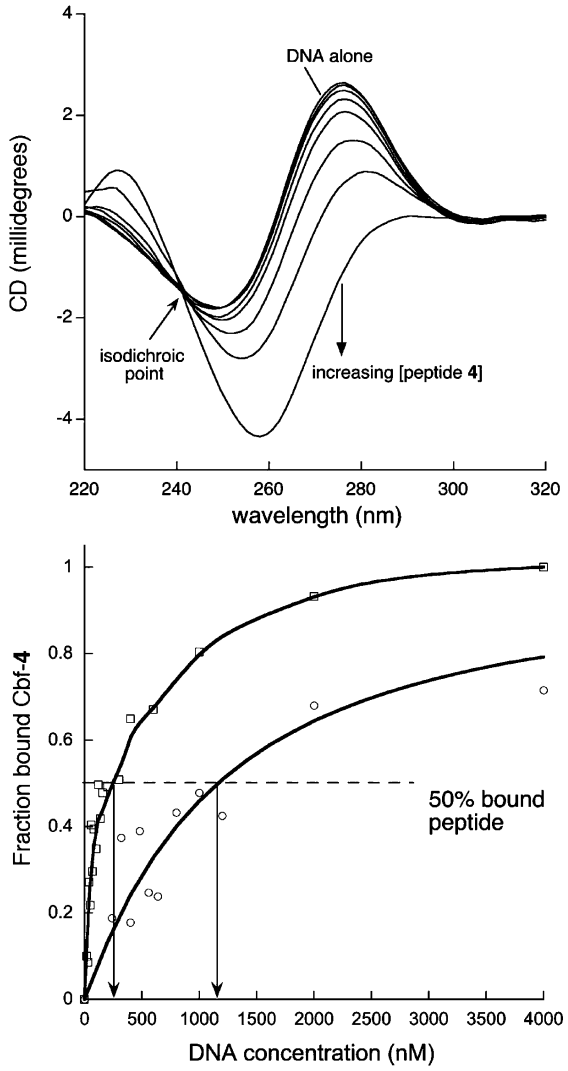

Figure 10. (Top) CD spectra of $dT_{15}C_4T_{15}$ with increasing Cbf-**4**, as indicated. Spectra with 0, 0.3, 0.6, 1.2, 2.5, 5, 10, and 20 μM peptide and 5 μM DNA are shown. (Bottom) Fluorescence anisotropy binding isotherms of Cbf-**4** with (○) $dT_4C_4T_4$ and (□) $dT_{15}C_4T_{15}$. A smoothed line is shown for $dT_{15}C_4T_{15}$, and a 1:1 fit to $dT_4C_4T_4$ is shown (R^2 = 0.96, K_d = 963 ± 129 nM).

drives assembly in a 1:1 $(EM^*)_4$ complex with $dT_4C_4T_4$, the quaternary 3:1 complex $[(\text{Cbf-}\mathbf{4})_3{\cdot}dT_{15}C_4T_{15}]$, which can bury 12 triplex stacks, exhibits strongly exothermic assembly. The DSC experiments were all run with the same concentration of $dT_{15}C_4T_{15}$ (25 μM), but the quaternary complex of $[((EM^*)_4)_3{\cdot}dT_{15}C_4T_{15}]$ was analyzed with 75 μM peptide. DSC analysis of the binary, lengthmatched $(EM^*)_4{\cdot}dT_4C_4T_4$ at similar higher concentrations did not yield detectable heats of assembly. Formation of the quaternary complex comes at a considerable entropic cost, exhibiting a T_m much lower than that of complexes with comparable dissociation enthalpy (Table 4). An estimation of 341 kcal/mol for the dissociation

Table 4. Dissociation Data for Heterotriplex $[\mathbf{10}{\cdot}\mathbf{4}{\cdot}dT_{15}C_4T_{15}]$[a]

peptide(s)	DNA	complex	T_m (°C)	ΔH_{DSC}
10	$dT_{15}C_4T_{15}$	1:1	56 (56)	+281/−303
4	$dT_{15}C_4T_{15}$	3:1	35 (27)	+110/−93
10 and **4**	$dT_{15}C_4T_{15}$	1:1:1	T_{m1} =25 (29)	+6/−4
			T_{m2} =56 (60)	+294/−313

[a]DNA concentration was 5 μM and 25 μM for UV and DSC measurements, respectively, with peptide ratios as indicated. Enthalpies from DSC are shown for upscan/downscan in kcal/mol. T_m's are shown as obtained by DSC and UV, shown in parentheses.

enthalpy of a $dT_{15}C_4T_{15}$ template fully saturated by melamine peptide binding could be obtained by summing ΔH_d for [ABA-**10**·$dT_{15}C_4T_{15}$] and [Cbf-**5**·$dT_5C_4T_5$], which is reasonably close to the measured ΔH_d for $[(\text{Cbf-}\mathbf{4})_3{\cdot}dT_{15}C_4T_{15}]$ of 330 kcal/mol DNA. Overall, cooperative assembly of ternary and quaternary bPNA–DNA complexes exhibit enthalpy and thermal stability gains relative to the length-matched bPNA–DNA heterodimers.

■ CONCLUSIONS

We find optimal bPNA–DNA complexation when the ratio of melamine to thymine bases is 1:2, consistent with interface length-matching selection. Although enthalpy–entropy compensation yielded a slow increase in K_d as the recognition interface was shortened, dissociation enthalpy and thermal stability exhibited strongly linear positive correlations with the number of melamine binding sites in the peptide and thymine

dx.doi.org/10.1021/bi4008963 | Biochemistry XXXX, XXX, XXX–XXX

content of the DNA interface. Complexation may thus be easily tuned by the length of the designed interface. Maximum binding efficacy was observed when the number of T−T hairpin sites and melamine peptide residues was the same, though a high number of mismatch sites and T−C/C−T half-sites were tolerated before complex T_m dropped below 37 °C (Table 2). As both DNA and peptide partner develop secondary structure on binding, complex formation is generally cooperative, with the entropic cost of folding paid for by the enthalpic benefit of base-stacking. A striking feature of this system is the high degree of cooperative multisite binding observed in the complexation of long T-tracts with short melamine peptides. This may be rationalized because the first peptide to bind folds thymine-rich DNA into a hairpin structure, aligning additional T−T sites for further melamine peptide binding, resulting in highly cooperative binding. Similar to turn nucleation,[58−65] the greatest entropic cost is expected to be associated with the initial formation of the dC_4 loop structure to allow antiparallel presentation of the two T-rich hairpin strands; base-stacking fails to compensate for this cost around four triplex repeat units of bPNA−DNA. More structured synthetic multivalent systems that have decoupled folding from binding are known to bind monovalent ligands independently rather than cooperatively.[66,67] Overall, the melamine−thymine recognition motif may be utilized to predictably prepare stable binary, ternary and quaternary macromolecular peptide−DNA complexes with thymine-rich single-stranded DNA. The structural simplicity and synthetic accessibility of the bPNA strand, coupled with its robust polythymidine recognition properties, raises the intriguing possibility that triazine-bearing macromolecules may used as biotechnology tools to direct the chemistry of native nucleic acids.

■ ASSOCIATED CONTENT

Ⓢ Supporting Information

Detailed synthetic procedures, compound and peptide characterization, additional fluorescence quenching titration data, complex melting curves. This material is available free of charge via the Internet at http://pubs.acs.org.

■ AUTHOR INFORMATION

Corresponding Author

*D. Bong. E-mail: bong@chem.osu.edu. Phone: (614) 247-8404.

Notes

The authors declare no competing financial interest.

■ ACKNOWLEDGMENTS

This work was supported The Ohio State University.

■ REFERENCES

(1) Felsenfeld, G., Davies, D. R., and Rich, A. (1957) Formation of a three-stranded polynucleotide molecule. *J. Am. Chem. Soc. 79*, 2023−2024.

(2) Chen, H., Meena, and McLaughlin, L. W. (2008) A Janus-Wedge DNA Triplex with A-W1-T and G-W2-C Base Triplets. *J. Am. Chem. Soc. 130*, 13190−13191.

(3) Soto, A. M., Loo, J., and Marky, L. A. (2002) Energetic contributions for the formation of TAT/TAT, TAT/CGC(+), and CGC(+)/CGC(+) base triplet stacks. *J. Am. Chem. Soc. 124*, 14355−14363.

(4) Moser, H. E., and Dervan, P. B. (1987) Sequence-specific cleavage of double helical DNA by triple helix formation. *Science 238*, 645−650.

(5) Le Doan, T., Perrouault, L., Praseuth, D., Habhoub, N., Decout, J.-L., Thuong, N. T., Lhomme, J., and Hélène, C. (1987) Sequence-specific recognition, photocrosslinking and cleavage of the DNA double helix by an oligo-[α]-thymidylate covalently linked to an azidoproflavine derivative. *Nucleic Acids Res. 15*, 7749−7760.

(6) Dervan, P. B., Doss, R. M., and Marques, M. A. (2005) Programmable DNA binding oligomers for control of transcription. *Curr. Med. Chem.: Anti-Cancer Agents 5*, 373−387.

(7) Hansen, M. E., Bentin, T., and Nielsen, P. E. (2009) High-affinity triplex targeting of double stranded DNA using chemically modified peptide nucleic acid oligomers. *Nucleic Acids Res. 37*, 4498−4507.

(8) Malnuit, V., Duca, M., and Benhida, R. (2011) Targeting DNA base pair mismatch with artificial nucleobases. Advances and perspectives in triple helix strategy. *Org. Biomol. Chem. 9*, 326−336.

(9) Zeng, Y., Pratumyot, Y., Piao, X., and Bong, D. (2012) Discrete assembly of synthetic peptide−DNA triplex structures from polyvalent melamine−thymine bifacial recognition. *J. Am. Chem. Soc. 134*, 832−835.

(10) Kool, E. T. (1997) Preorganization of DNA: Design Principles for Improving Nucleic Acid Recognition by Synthetic Oligonucleotides. *Chem. Rev. 97*, 1473−1488.

(11) Branda, N., Kurz, G., and Lehn, J.-M. (1996) Janus wedges: a new approach towards nucleobase-pair recognition. *Chem. Commun. 1996*, 2443−2444.

(12) Shin, D., and Tor, Y. (2011) Bifacial Nucleoside as a Surrogate for Both T and A in Duplex DNA. *J. Am. Chem. Soc. 133*, 6926−6929.

(13) Fenniri, H., Packiarajan, M., Vidale, K. L., Sherman, D. M., Hallenga, K., Wood, K. V., and Stowell, J. G. (2001) Helical rosette nanotubes: Design, self-assembly, and characterization. *J. Am. Chem. Soc. 123*, 3854−3855.

(14) Nielsen, P. E., Egholm, M., Berg, R. H., and Buchardt, O. (1991) Sequence-selective recognition of DNA by strand displacement with a thymine-substituted polyamide. *Science 254*, 1497−1500.

(15) Betts, L., Josey, J. A., Veal, J. M., and Jordan, S. R. (1995) A nucleic acid triple helix formed by a peptide nucleic acid-DNA complex. *Science 270*, 1838−41.

(16) Bentin, T., Larsen, H. J., and Nielsen, P. E. (2003) Combined Triplex/Duplex Invasion of Double-Stranded DNA by "Tail-Clamp" Peptide Nucleic Acid. *Biochemistry 42*, 13987−13995.

(17) Kaihatsu, K., Shah, R. H., Zhao, X., and Corey, D. R. (2003) Extending Recognition by Peptide Nucleic Acids (PNAs): Binding to Duplex DNA and Inhibition of Transcription by Tail-Clamp PNA-Peptide Conjugates. *Biochemistry 42*, 13996−14003.

(18) Doluca, O., Withers, J. M., and Filichev, V. V. (2013) Molecular Engineering of Guanine-Rich Sequences: Z-DNA, DNA Triplexes, and G-Quadruplexes. *Chem. Rev. 113*, 3044−3083.

(19) Datta, B., Schmitt, C., and Armitage, B. A. (2003) Formation of a PNA2-DNA2 hybrid quadruplex. *J. Am. Chem. Soc. 125*, 4111−4118.

(20) Datta, B., Bier, M. E., Roy, S., and Armitage, B. A. (2005) Quadruplex Formation by a Guanine-Rich PNA Oligomer. *J. Am. Chem. Soc. 127*, 4199−4207.

(21) Deigan, K. E., and Ferré-D,'Amaré, A. R. (2011) Riboswitches: discovery of drugs that target bacterial gene-regulatory RNAs. *Acc. Chem. Res. 44*, 1329−1338.

(22) Smith, A. M., Fuchs, R. T., Grundy, F. J., and Henkin, T. (2010) Riboswitch RNAs: Regulation of gene expression by direct monitoring of a physiological signal. *RNA Biol. 7*, 104−110.

(23) Topp, S., and Gallivan, J. P. (2010) Emerging Applications of Riboswitches in Chemical Biology. *ACS Chem. Biol. 5*, 139−148.

(24) Zhang, W., Nowlan, D. T., Thomson, L. M., Lackowski, W. M., and Simanek, E. E. (2001) Orthogonal, Convergent Syntheses of Dendrimers Based on Melamine with One or Two Unique Surface Sites for Manipulation. *J. Am. Chem. Soc. 123*, 8914−8922.

(25) Blotny, G. (2006) Recent applications of 2, 4, 6-trichloro-1, 3, 5-triazine and its derivatives in organic synthesis. *Tetrahedron 62*, 9507−9522.

(26) Chen, H.-T., Neerman, M. F., Parrish, A. R., and Simanek, E. E. (2004) Cytotoxicity, Hemolysis, and Acute in Vivo Toxicity of Dendrimers Based on Melamine, Candidate Vehicles for Drug Delivery. *J. Am. Chem. Soc. 126*, 10044−10048.
(27) Leman, L., Orgel, L., and Ghadiri, M. R. (2004) Carbonyl sulfide-mediated prebiotic formation of peptides. *Science 306*, 283−286.
(28) Li, X., and Liu, D. R. (2004) DNA-templated organic synthesis: nature's strategy for controlling chemical reactivity applied to synthetic molecules. *Angew. Chem., Int. Ed. Engl. 43*, 4848−4870.
(29) Nielsen, P. E. (2007) Peptide Nucleic Acids and the Origin of Life. *Chem. Biodiversity 4*, 1996−2002.
(30) Ura, Y., Beierle, J. M., Leman, L. J., Orgel, L. E., and Ghadiri, M. R. (2009) Self-assembling sequence-adaptive peptide nucleic acids. *Science 325*, 73−77.
(31) Hysell, M., Siegel, J. S., and Tor, Y. (2005) Synthesis and stability of exocyclic triazine nucleosides. *Org. Biomol. Chem. 3*, 2946−2952.
(32) Mittapalli, G. K., Osornio, Y. M., Guerrero, M. A., Reddy, K. R., Krishnamurthy, R., and Eschenmoser, A. (2007) Mapping the landscape of potentially primordial informational oligomers: oligodipeptides tagged with 2,4-disubstituted 5-aminopyrimidines as recognition elements. *Angew. Chem., Int. Ed. 46*, 2478−2484.
(33) Mittapalli, G. K., Reddy, K. R., Xiong, H., Munoz, O., Han, B., De Riccardis, F., Krishnamurthy, R., and Eschenmoser, A. (2007) Mapping the landscape of potentially primordial informational oligomers: oligodipeptides and oligodipeptoids tagged with triazines as recognition elements. *Angew. Chem., Int. Ed. 46*, 2470−2477.
(34) Ferris, J. P., Sanchez, R. A., and Orgel, L. E. (1968) Studies in prebiotic synthesis: III. Synthesis of pyrimidines from cyanoacetylene and cyanate. *J. Mol. Biol. 33*, 693−704.
(35) Menor-Salván, C., Ruiz-Bermejo, D., Guzmán, M. I., Osuna-Esteban, S., and Veintemillas-Verdaguer, S. (2009) Synthesis of pyrimidines and triazines in ice: implications for the prebiotic chemistry of nucleobases. *Chem.—Eur. J. 15*, 4411−4418.
(36) Whitesides, G. M., Simanek, E. E., Mathias, J. P., Seto, C. T., Chin, D., Mammen, M., and Gordon, D. M. (1995) Noncovalent Synthesis: Using Physical-Organic Chemistry To Make Aggregates. *Acc. Chem. Res. 28*, 37−44.
(37) ten Cate, M. G. J., Huskens, J., Crego-Calama, M., and Reinhoudt, D. N. (2004) Thermodynamic stability of hydrogen-bonded nanostructures: A calorimetric study. *Chem.—Eur. J. 10*, 3632−3639.
(38) Prins, L. J., Reinhoudt, D. N., and Timmerman, P. (2001) Noncovalent synthesis using hydrogen bonding. *Angew. Chem., Int. Ed. 40*, 2382−2426.
(39) Oshovsky, G. V., Reinhoudt, D. N., and Verboom, W. (2007) Supramolecular chemistry in water. *Angew. Chem., Int. Ed. 46*, 2366−2393.
(40) De Greef, T. F. A., Smulders, M. M. J., Wolffs, M., Schenning, A., Sijbesma, R. P., and Meijer, E. W. (2009) Supramolecular Polymerization. *Chem. Rev. 109*, 5687−5754.
(41) Cafferty, B. J., Gállego, I., Chen, M. C., Farley, K. I., Eritja, R., and Hud, N. V. (2013) Efficient Self-Assembly in Water of Long Noncovalent Polymers by Nucleobase Analogues. *J. Am. Chem. Soc. 135*, 2447−2450.
(42) Ai, K., Liu, Y., and Lu, L. (2009) Hydrogen-Bonding Recognition-Induced Color Change of Gold Nanoparticles for Visual Detection of Melamine in Raw Milk and Infant Formula. *J. Am. Chem. Soc. 131*, 9496−9497.
(43) Kawasaki, T., Tokuhiro, M., Kimizuka, N., and Kunitake, T. (2001) Hierarchical self-assembly of chiral complementary hydrogen-bond networks in water: reconstitution of supramolecular membranes. *J. Am. Chem. Soc. 123*, 6792−6800.
(44) Ariga, K., and Kunitake, T. (1998) Molecular Recognition at Air-Water and Related Interfaces: Complementary Hydrogen Bonding and Multisite Interaction. *Acc. Chem. Res. 31*, 371−378.
(45) Marchi-Artzner, V., Gulik-Krzywicki, T., Guedeau-Boudeville, M.-A., Gosse, C., Sanderson, J. M., Dedieu, J.-C., and Lehn, J.-M. (2001) Selective adhesion, lipid exchange and membrane-fusion processes between vesicles of various sizes bearing complementary molecular recognition groups. *ChemPhysChem 2*, 367−376.
(46) Zhou, Z., and Bong, D. (2013) Small-Molecule/Polymer Recognition Triggers Aqueous-Phase Assembly and Encapsulation. *Langmuir 29*, 144−150.
(47) Ma, M., and Bong, D. (2011) Directed peptide assembly at the lipid-water interface cooperatively enhances membrane binding and activity. *Langmuir 27*, 1480−1486.
(48) Ma, M., and Bong, D. (2011) Determinants of cyanuric acid and melamine assembly in water. *Langmuir 27*, 8841−8853.
(49) Ma, M., and Bong, D. (2011) Protein assembly directed by synthetic molecular recognition motifs. *Org. Biomol. Chem. 9*, 7296−7299.
(50) Ma, M., Gong, Y., and Bong, D. (2009) Lipid Membrane Adhesion and Fusion Driven by Designed, Minimally Multivalent Hydrogen-Bonding Lipids. *J. Am. Chem. Soc. 131*, 16919−16926.
(51) Ma, M., Paredes, A., and Bong, D. (2008) Intra- and intermembrane pairwise molecular recognition between synthetic hydrogen-bonding phospholipids. *J. Am. Chem. Soc. 130*, 14456−8.
(52) Jahromi, A. H., Nguyen, L., Fu, Y., Miller, K. A., Baranger, A. M., and Zimmerman, S. C. (2013) A Novel CUG^{exp}-MBNL1 Inhibitor with Therapeutic Potential for Myotonic Dystrophy Type 1. *ACS Chem. Biol. 8*, 1037−1043.
(53) Arambula, J. F., Ramisetty, S. R., Baranger, A. M., and Zimmerman, S. C. (2009) A simple ligand that selectively targets CUG trinucleotide repeats and inhibits MBNL protein binding. *Proc. Natl. Acad. Sci. U. S. A. 106*, 16068−16073.
(54) SantaLucia, J., Jr., and Hicks, D. (2004) The thermodynamics of DNA structural motifs. *Annu. Rev. Biophys. Biomol. Struct. 33*, 415−40.
(55) Kool, E. T. (2003) Hydrogen bonding, base stacking and steric effects in DNA replication. *Ann. Rev. Biophys. Biomol. Struct. 30*, 1−22.
(56) Gilli, P., Ferretti, V., Gilli, G., and Borea, P. A. (1994) Enthalpy-entropy compensation in drug-receptor binding. *J. Phys. Chem. 98*, 1515−1518.
(57) Dunitz, J. D. (1995) Win some, lose some: enthalpy-entropy compensation in weak intermolecular interactions. *Chem. Biol. 2*, 709−712.
(58) Ghadiri, M. R., and Choi, C. (1990) Secondary structure nucleation in peptides. Transition metal ion stabilized .alpha.-helices. *J. Am. Chem. Soc. 112*, 1630−1632.
(59) Ghadiri, M. R., and Fernholz, A. K. (1990) Peptide architecture. Design of stable .alpha.-helical metallopeptides via a novel exchange-inert ruthenium(III) complex. *J. Am. Chem. Soc. 112*, 9633−9635.
(60) Cabezas, E., and Satterthwait, A. C. (1999) The hydrogen bond mimic approach: solid-phase synthesis of a peptide stabilized as an .alpha.-helix with a hydrazone link. *J. Am. Chem. Soc. 121*, 3862−3875.
(61) Ruan, F., Chen, Y., Itoh, K., Sasaki, T., and Hopkins, P. B. (1991) Synthesis of peptides containing unnatural, metal-ligating residues: aminodiacetic acid as a peptide side chain. *J. Org. Chem. 56*, 4347−54.
(62) Schafmeister, C. E., Po, J., and Verdine, G. L. (2000) An All-Hydrocarbon Cross-Linking System for Enhancing the Helicity and Metabolic Stability of Peptides. *J. Am. Chem. Soc. 122*, 5891−5892.
(63) Chapman, R. N., Dimartino, G., and Arora, P. S. (2004) A Highly Stable Short alpha-Helix Constrained by a Main-Chain Hydrogen-Bond Surrogate. *J. Am. Chem. Soc. 126*, 12252−12253.
(64) Torres, O., Yuksel, D., Bernardina, M., Kumar, K., and Bong, D. (2008) Peptide tertiary structure nucleation by side-chain crosslinking with metal complexation and double "click" cycloaddition. *ChemBioChem 9*, 1701−1705.
(65) Gellman, S. H. (1998) Minimal model systems for β-sheet secondary structure in proteins. *Curr. Opin. Chem. Biol. 2*, 717−725.
(66) Mammen, M., Choi, S.-K., and Whitesides, G. M. (1998) Polyvalent Interactions in Biological Systems: Implications for Design and Use of Multivalent Ligands and Inhibitors. *Angew. Chem., Int. Ed. 37*, 2754−2794.

dx.doi.org/10.1021/bi4008963 | *Biochemistry* XXXX, XXX, XXX−XXX

(67) Rao, J., Lahiri, J., Isaacs, L., Weis, R. M., and Whitesides, G. M. (1998) A trivalent system from vancomycin.D-ala-D-Ala with higher affinity than avidin-biotin. *Science 280*, 708−11.

dx.doi.org/10.1021/bi4008963 | *Biochemistry* XXXX, XXX, XXX−XXX